Ibn Al-Haitham Journal for Pure and Applied Sciences
Journal homepage: jih.uobaghdad.edu.iq
PISSN: 1609-4042, EISSN: 2521-3407
IHJPAS. 2025, 38 (1)

# Assessing Landsat Processing Levels and Support Vector Machine Classification

**Nehad Hameed[1*] and Taghreed A. Naji[2]**

[1,2] Department of Physics, College of Education for Pure Science (Ibn Al-Haitham), University of Baghdad, Baghdad, Iraq.

*Corresponding Author.

Received: 27 April 2024 Accepted: 24 July 2024 Published: 20 January 2025

**doi.org/10.30526/38.1.3992**

## Abstract

The availability of different processing levels for satellite images makes it important to measure their suitability for classification tasks. This study investigates the impact of the Landsat data processing level on the accuracy of land cover classification using a support vector machine (SVM) classifier. The classification accuracy values of Landsat 8 (LS8) and Landsat 9 (LS9) data at different processing levels vary notably. For LS9, Collection 2 Level 2 (C2L2) achieved the highest accuracy of (86.55%) with the polynomial kernel of the SVM classifier, surpassing the Fast Line-of-Sight Atmospheric Analysis of Spectral Hypercubes (FLAASH) at (85.31%) and Collection 2 Level 1 (C2L1) at (84.93%). The LS8 data exhibits similar behavior. Conversely, when using the maximum-likelihood classifier, the highest accuracy (83.06%) was achieved with FLAASH. The results demonstrate significant variations in accuracies for different land cover classes, which emphasizes the importance of per-class accuracy. The results highlight the critical role of preprocessing techniques and classifier selection in optimizing the classification processes and land cover mapping accuracy for remote sensing geospatial applications. Finally, the actual differences in classification accuracy between processing levels are larger than those given by the confusion matrix. So, the consideration of alternative evaluation methods with the absence of reference images is critical.

**Keywords:** Support vector machine, remote sensing, atmospheric correction, Landsat 9, classification.

## 1. Introduction

Land use/ land cover (LU/LC) information plays a crucial role in various geospatial applications (1,2) . Satellite sensors are considered the most important source of information about the Earth's surface (3). It offers comprehensive insights into Earth’s features with notable promptness. With this remote-sensing (RS) system, a digital image is represented by intensity

values termed Digital Numbers (DN). These DNs serve as primary pixel values before conversion through absolute radiometric calibration into physical units, such as top-of-atmosphere (TOA) radiance or reflectance. This represents the initial phase in utilizing remote sensing data for quantitative analyses (4,5) by applying atmospheric correction (AC) to remove the effects of absorption and scattering due to atmospheric influences (6-8).

Landsat (LS) satellite images are broadly employed for land cover classification (9). With its global datasets, it holds significant potential for enhancing land surface classification (10). The United States Geological Survey (USGS) worked to ensure consistent processing levels for all the LS satellite series by introducing collections-based processing levels for the entire LS series archive, starting with Collection 1 (C1) in 2016. After launching Landsat 9 (LS9), Collection 2 (C2) was introduced in 2020 to reprocess all the LS archives with enhanced geo-referencing and offer a global catalog of surface reflectance (SR) and temperature (ST) under Level 2 (L2) products. C2 products cover all LS data, including the Operational Land Imagers (OLI 1 and 2) and Thermal Infrared (TIRS 1 and 2) sensors of LS8 and LS9, providing calibrated and geo-located Level 1 and 2 products (11).

The C2L1 and C2L2 data products store spectral band information as DNs with unsigned 16-bit integers, which can be transformed into units with physical meaning, such as the top of the atmospheric spectral reflectance or radiance, employing offset values and scale factors specific for each band stored in the metadata related to the products. The TOA reflectance and TOA radiance at Level 1 (L1) were calculated assuming that the solar zenith angle was equal to 0° and could be adjusted using the actual solar zenith angle provided in the product metadata. For Landsat 4–9, the solar and view angles are provided for each 30 m pixel in the metadata of the C2L1 product (13).

The Landsat Level-1 TOA reflectance is atmospherically corrected to the Level-2 Collection-2 Surface Reflectance (L2C2 SR) product by employing the LaSRC algorithm globally to perform atmospheric correction to enhance the SR accuracy(12,13). The FLAASH algorithm is widely used atmospheric correction software to facilitate the analysis of hyperspectral and multispectral imaging sensors operating in the visible and shortwave IR (Vis-SWIR) spectral ranges (14,15).

The use of robust classification algorithms is fundamental to remote sensing applications and essential for satellite image classification because of the spectral similarity among different surface types (16-18). The SVM has emerged as a popular nonparametric supervised classification method for digital image classification, capable of handling nonlinear classification situations using a limited number of samples (19,20). The SVM approach, based on the theory of statistical learning, detects decision boundaries that optimize the image classes' separation (21,22). Compared to many existing classifiers, the SVM classifier can achieve competitive results even with small training samples (23,24).

Several studies have investigated the effect of preprocessing levels and atmospheric corrections on the classification accuracy of satellite data. Chinsu Lin et al. (2015) (25) discovered that the AC at a 2 m spatial resolution does not appear to impact the classification accuracy of (LU/LC) using WorldView-2 multispectral imagery. In contrast, Jesús A., et al. (2018) (26) explored the impact of different preprocessing techniques, such as radiometric calibration and atmospheric correction on land use classification accuracy. Their results highlighted the importance of careful preprocessing to improve the classification results. A study by Lhissou, Rachid, et al. (2020) (27), subjected Landsat 8 images to image-based and physical atmospheric correction algorithms to evaluate their influences on the geological mapping accuracy. Their results evaluations were based

on the Spectro radiometric data collected by the ASD (Analytical Spectral Devices) and the overall accuracy result from the SVM. They compared the DOS1 image-based and (FLAASH and ATCOR) physical atmospheric correction algorithms, where FLAASH provided the most accurate reflectance estimation, slightly outperforming DOS1. The study showed image-based efficiency in atmospheric correction in dry and semi-dry areas, proving to be accurate, simple, and straightforward. The study conducted by J. Dohski et al. (2022) (28) evaluated the effects of atmospheric correction and image fusion methods on land cover classification accuracy using Landsat 8 imagery. They employed SVM and ML algorithms and found that SVM outperformed ML, achieving higher overall accuracy (OA) with various fusion techniques. Their results indicated that fusion methods enhanced classification accuracy, while atmospheric correction was deemed unnecessary for land cover mapping based on DN images.

Muchsin, Fadila, et al. (2023) (14) investigated the impact of various atmospheric correction algorithms, including FLAASH, on the classification accuracy of Landsat 8 C2L1 data. They compared these results with those obtained from C2L2 surface reflectance (SR) preprocessed by the data provider. Their results revealed that FLAASH consistently outperforms other algorithms, including the LaSRC method used by the data provider.

Understanding the influence of the Landsat preprocessing levels on the SVM classification results is crucial for optimizing the land cover mapping accuracy. By leveraging advanced preprocessing techniques and robust classification algorithms like SVM, researchers can enhance the reliability and utility of remote sensing data for land cover classification applications.

This paper investigates the impact of different Landsat (OLI) data processing levels (Collection 2, Level 1 TOA, and Level 2 SR) and FLAASH atmospheric correction on the land cover classification results obtained using the Support Vector Machine (SVM) algorithm. Additionally, this research assesses the efficacy and robustness of SVM classification for handling different processing levels, including atmospheric corrections and radiometric calibrations, focusing on improving classification performance for geospatial applications, such as land use mapping and environmental monitoring.

## 2. Materials and Methods

### 2.1 Used Data

This study utilized satellite imagery from Landsat 8 OLI1/TIRS C2 L1, C2 L2, and Landsat 9 OLI2/TIRS with the same processing levels. The Landsat OLI C2 L2 collection provides global surface reflectance data, whereas the C2 L2 products provide TOA data (29,30). The satellite scenes where the used data were extracted are identified by LANDSAT_PRODUCT_IDs = "LC08_L1TP_168037_20240114_20240114_02_T1", "LC08_L2SP_168037_20240114_20240123_02_T1",**"**LC09_L1TP_168037_20240106_20240106_02_T1", and "LC09_L2TP_168037_20240106_20240107_02_T1". The Landsat 8/9 satellites have two instruments: OLI 1 and 2 and the TIRS 1 and 2. The OLI consists of 11 channels (dynamic range 16-bit), with the first seven channels being multispectral (visible, near-infrared, and shortwave infrared) registered at a spatial resolution of 30 m. TIRS-2 consists of two thermal infrared channels with a spatial resolution of 100 m (31-36). All data were collected from the OLI1/2 sensors. **Table 1** lists the Landsat satellite data for path 168 and row

037, along with the accusation dates and the range of the study area. The remotely sensed images were downloaded from the USGS website (https://earthexplorer.usgs.gov/).

**Table 1.** The satellite scenes used in this study.

| Satellite Scene | Processing level | Date | GMT acquisition time (a.m.) | Scene area km$^2$ |
|---|---|---|---|---|
| Landsat 8 OLI | C2L1<br>C2L2 | 14 January 2024 | 07:33:50 | 900 |
| Landsat 9 OLI2 | C2L1<br>C2 L2 | 6 January 2024 | 07:33:45 | 900 |

## 2.2 Methods

Four satellite scenes were used for the same region: the first pair consisted of Landsat 9 OLI2 sensor data at Level 1 (C2L1) (TOA) and Level 2 (C2L2) (SR), while the second pair comprised Landsat 8 OLI1 data processed at the same processing levels. Following the clipping of the study area from the original scenes. Band stacking was performed for all four study area scenes clipped from the original scenes. Radiometric calibration (37) and FLAASH atmospheric correction was applied to the two C2L1 scenes. Subsequently, six scenes (two original (C2L1), two C2L2, and two level-1 FLAASH-corrected scenes) were subjected to SVM and ML classifiers to evaluate the influence of atmospheric correction on the classification accuracy. **Figure 1** shows the procedural workflow used in this study.

The eight classes (shaded, crops, non-residential, palm and trees, bare lands, water bodies, natural vegetation, and urban) were chosen for the study site indicated in **Figure 4**. To identify these classes and training sets selection, a field survey was conducted, supplemented by a study of various satellite scenes beyond those from Landsat 8 and 9. These additional satellite scenes were studied to enhance the understanding of the study site characteristics and land cover types, thereby aiding in the accurate identification and selection of training sets for the classification process. The classification's overall accuracy (OA) was measured using Eq. (1) and the confusion matrix (38,39).

$$OA = \frac{Number\ of\ right\ classified}{Total\ \ pixels\ number} \times 100\ \% \quad (1)$$

SNAP 6.0.0 software was used to read the original scenes and clip the study site. The other work steps were conducted using ENVI 5.6.1 software. The Landsat data provider applies the LaSRC algorithm to correct C2L1 to C2L2.

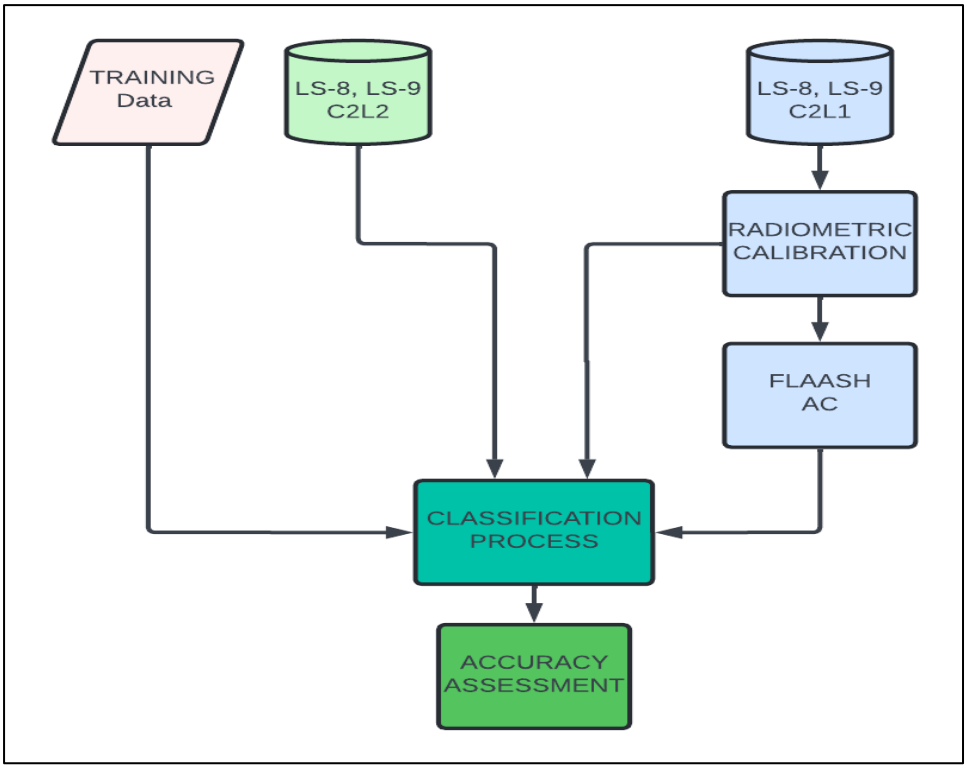


**Figure 1**. The workflow diagram

### 2.3 Study Site

The chosen study site for this investigation lies between latitudes 36° 69' 87.0" N to 36° 99' 87.0" N and longitudes 42° 78' 90.0" E to 45° 78' 90.0" E, covering an area of 900 square kilometers. The main part of the study area is Baghdad, Iraq's capital. This urban center is densely populated with limited green spaces and open land; some of which are covered with various types of natural vegetation. The Tigris River crosses Baghdad city, dividing it into two sections (on the west bank of Al-Karkh, while Al-Rusafa represents the east part) (40) and converges with the Diyala River in the southern region (41). The study area encompasses additional geographical features such as smaller streams, canals, and man-made lakes. The surrounding area consists of agricultural land, including greenery with palm groves, wheat and barley fields, fodder crops, and various orchards scattered across smaller parcels of land. Urban development in these zones exhibits a low population density. In the western sector of the study area lies Baghdad International Airport. The elevation of the study site above sea level is approximately 31-39 m (42). The land use composition in the study region varies, including industrial zones, commercial areas, and transportation infrastructure. **Figure 2** shows the original Landsat 9 scene and the study area.

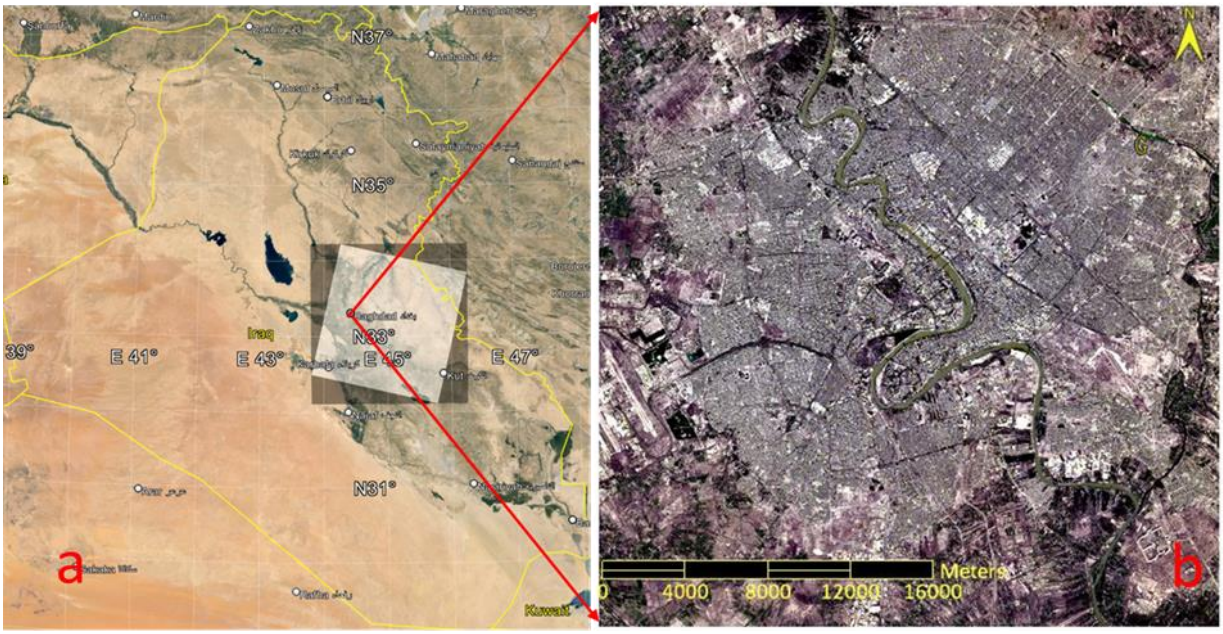


**Figure 2.** a. Iraqi country map with Landsat 9 satellite scene (path 168, and row 37), b- the natural color scene of the clipped study site.

## 3. Results and Discussion

**Figure 3** presents six scenes before and after conducting FLAASH atmospheric correction for the C2L1 scenes of LS8, LS9, and the C2L2 scenes of both satellites.

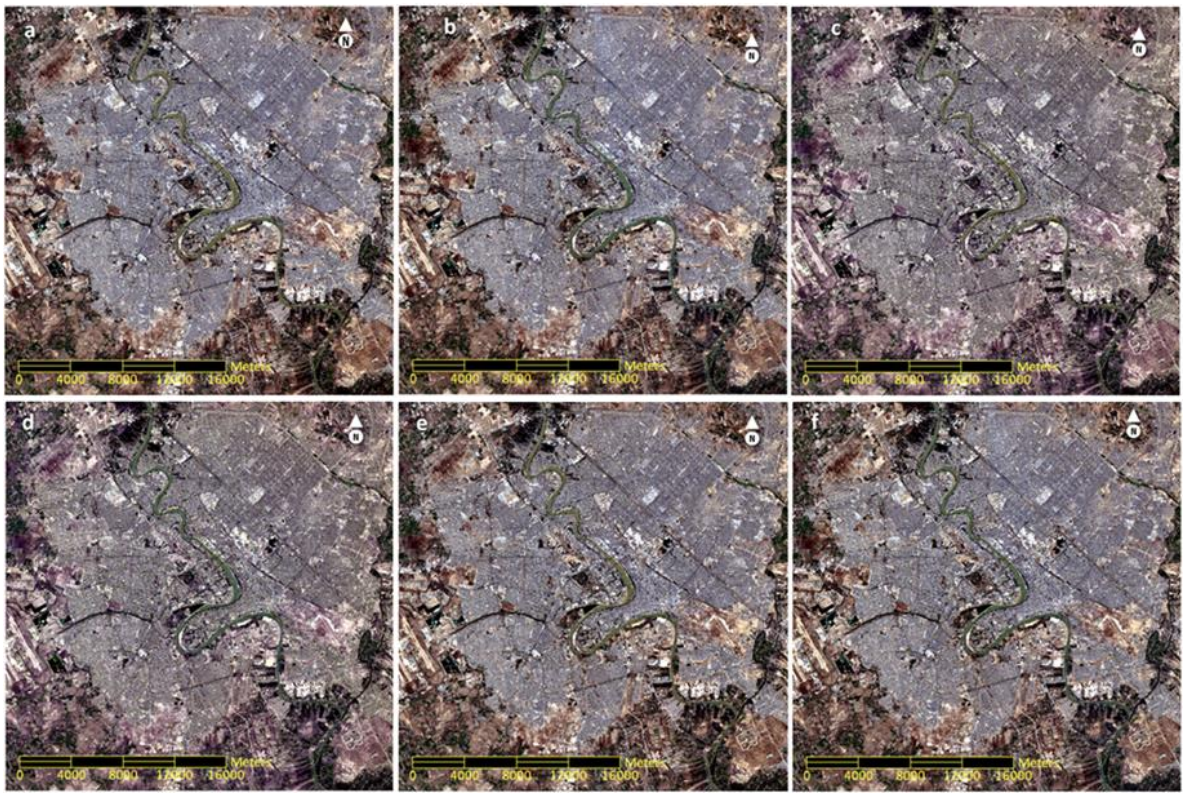


**Figure 3.** a- LS9C2L1, b-LS9C2L2, c-LS9FLAASH, d-LS8C2L1, e- LS8C2L2, and f- LS8FLAASH.

**Table 2** presents the classification results for different processing levels and classifiers, with noteworthy differences in overall accuracies and more significant disparities in detailed accuracies shown in **Table 3** Overall, the accuracy increased with higher processing levels, particularly for LS8C2L2 and LS9C2L2, indicating the crucial role of atmospheric correction and preprocessing techniques in enhancing classification performance.

**Table 1.** Classification's overall accuracy results for different classification algorithms and processing levels

| CLASSIFIER | LS8C2L1 | LS8C2L2 | LS8FLAASH | LS9C2L1 | LS9C2L2 | LS9FLAASH |
|---|---|---|---|---|---|---|
| SVM LIN | 84 | 85.07 | 84.53 | 84.97 | 86.29 | 85.46 |
| SVM RBF | 84.1 | 85.25 | 84.62 | 84.88 | 86.43 | 85.19 |
| SVM PO | 84.03 | 85.14 | 84.48 | 84.93 | 86.55 | 85.31 |
| ML | 82.56 | 82.85 | 82.91 | 82.71 | 82.74 | 83.06 |

When comparing the classification results in **Table 2** for the corrected images (FLAASH and C2L2) and the results of C2L1, the FLAASH-corrected images exhibited greater improvement with the linear (LIN) kernel across both satellites, with a slight difference compared to the other kernels. For the C2L2-corrected images, the RBF kernel provided the highest improvement with the LS8 satellite, while the polynomial (PO) kernel yielded the best results with the LS9 satellite. Overall, the SVM classifier demonstrated the best performance with C2L2 images. However, the Maximum Likelihood (ML) classifier, with the FLAASH-corrected images, demonstrated a minimal performance increase over the C2L2 images for both satellites. The LaSRC algorithm is superior to the FLAASH algorithm, when coupled with SVM classifiers. Specifically, the SVM PO classifier improved from LS8C2L1 (84.03%) to LS8C2L2 (85.14%), LS8FLAASH (84.48%), LS9C2L1 (84.93%), LS9C2L2 (86.55%), and LS9FLAASH (85.31%). This demonstrates the impact of atmospheric correction on the SVM-based classification algorithms. The ML classifier exhibits stable accuracies across different processing levels, with fluctuations of less than 0.35%, without significant variations in performance with various datasets. **Figure 4** shows the classification results for the SVM LIN LS9C2L1, SVM LINLS9C2L2, SVM PO LS9C2L1, SVM PO LS9C2L2, ML LS9C21, and LS9FLAASH.

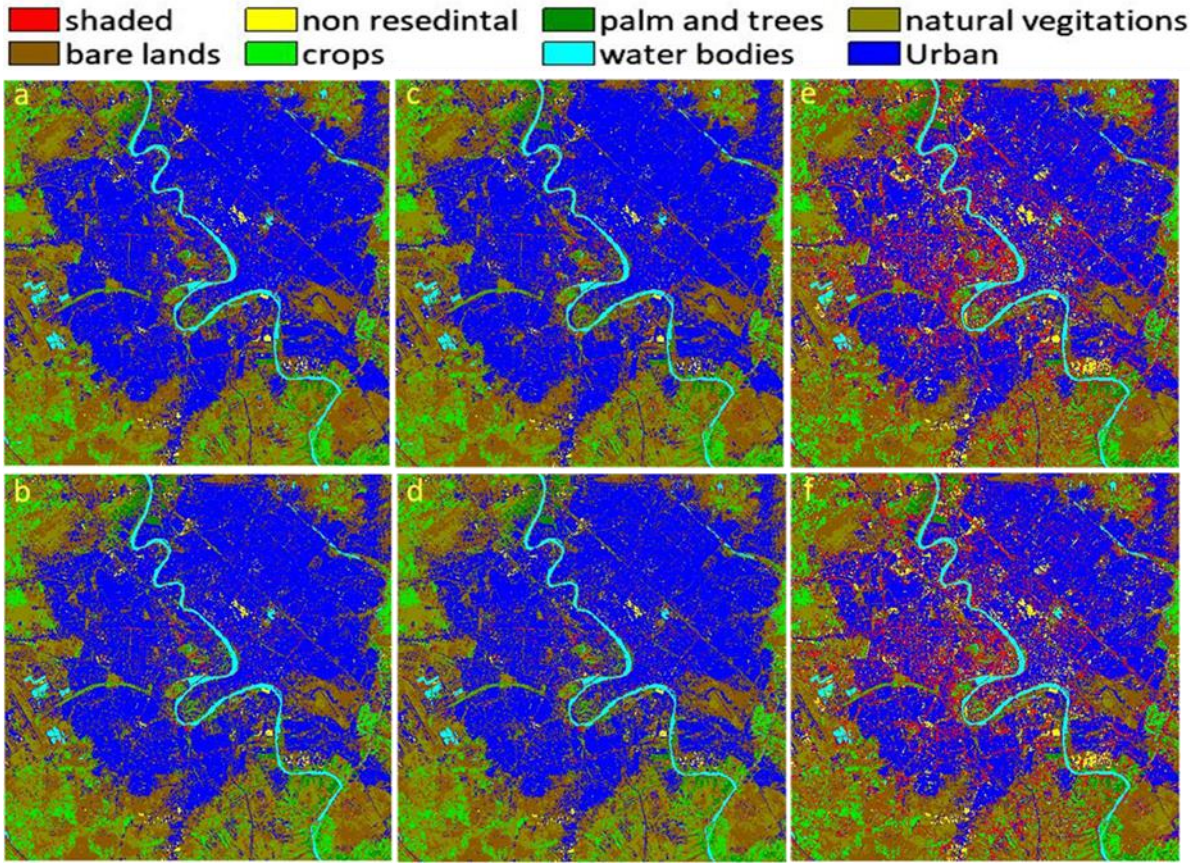


**Figure 4**. Classification result a- LIN-LS9C2L1, b- LIN-LS9C2L2, c- PO-LS9C2L1, d- PO-LS9C2L2 e- ML-LS9C2L1, and f- ML-LS9FLAASH.

Despite minor differences in overall accuracy, significant variations exist in the accuracy of land cover classes with different classifiers and processing levels. **Table 3** presents the producer accuracy (Prod. Acc.) and user accuracy (User Acc.) for the SVM linear kernel (LIN) at two processing levels (C2L1 and C2L2) of LS9 data, as well as for ML with C2L1 and FLAASH-corrected scenes.

**Table 2.** User and producer accuracy for some classification results and different datasets.

| | **LIN LS9C2L1** | | **LIN LS9C2L2** | | **ML-LS9C2L1** | | **ML-LS9FLAASH** | |
|---|---|---|---|---|---|---|---|---|
| **Class** | **Prod. Acc.** | **User Acc.** | **Prod. Acc.** | **User Acc.** | **Prod. Acc.** | **User Acc.** | **Prod. Acc.** | **User Acc.** |
| Shaded | 55.77 | 90.63 | 59.62 | 93.75 | 58.85 | 61.28 | 61.03 | 63.81 |
| Crops | 92.35 | 98.07 | 93.99 | 96.81 | 91.8 | 88.11 | 94.72 | 84.42 |
| Non-Residential | 82.94 | 98.05 | 82.39 | 97.72 | 96.42 | 85.59 | 95.46 | 84.84 |
| Palms and Trees | 76.55 | 98.23 | 75.98 | 97.78 | 71.38 | 96.13 | 70.23 | 98.07 |
| Bare Lands | 89.85 | 71.78 | 92.77 | 78.01 | 81.92 | 72.72 | 81.5 | 73.34 |
| Water Bodies | 99.3 | 88.82 | 99.07 | 89.36 | 99.42 | 90.72 | 99.42 | 91.11 |
| Natural Vegetation | 86.63 | 86.31 | 90.29 | 82.11 | 77.3 | 97.92 | 78.94 | 97.81 |
| Urban | 93.45 | 72.8 | 94.1 | 75.73 | 86.01 | 77.61 | 85.77 | 78.3 |

In **Table 3**, there are varying levels of user accuracy (User Acc.) and producer accuracy (Prod.

Acc.), results obtained for different land cover classes and classifiers. The main observations are summarized:

- Shaded Areas: The SVM classifier with LS9C2L1 and LS9C2L2 outperforms the ML classifier in terms of both producer and user accuracy, with LS9C2L2 showing higher accuracy.
- Crops class: The SVM classifier with LS9C2L1 exhibits slightly higher producer accuracy compared to LS9C2L2, while the ML classifier shows lower accuracy.
- Non-Residential Areas: The ML classifier consistently outperformed the SVM classifier in terms of both producer and user accuracy across both processing levels.
- Palm and Trees: Both classifiers performed well, with slightly higher accuracy observed for LS9C2L1 compared to LS9C2L2.
- Bare Lands: The SVM classifier with LS9C2L2 showed higher producer accuracy compared to LS9C2L1, while user accuracy was slightly higher for LS9C2L1. The ML classifier showed a more balanced performance between the two processing levels.
- Water Bodies: Both classifiers performed exceptionally well, and very high accuracies were observed across both processing levels.
- Natural Vegetation: The SVM classifier LS9C2L2 demonstrated higher producer accuracy compared to LS9C2L1, while user accuracy was slightly higher for LS9C2L1. The ML classifier exhibits similar trends but with slightly lower accuracy compared to the SVM classifier.
- Urban areas. Both classifiers showed high accuracy, with LS9C2L1 showing slightly higher accuracy compared to LS9C2L2 for both producer and user accuracy.

The SVM classifier performs better in terms of producer accuracy, especially at the LS9C2L2 processing level, whereas the ML classifier shows more consistent performance with different land cover classes and processing levels. There are some variations in accuracy metrics between processing levels. Careful consideration is important when selecting classifiers and processing levels for remote sensing classification tasks.

The variations in the results listed in **Table 2** and **Table 3** do not match the variations observed visually and by other means of comparison. For example, the difference in OA between the LS9C2L2 and LS9C2L1 images was 1.62% with the polynomial kernel and 1.52% with the RBF kernel. In contrast, the real difference between them (for comparison, one of them is used as a ground truth image) amounts to 14.2% for both kernels. When using ML to classify the same image, the difference in OA was less than 0.3%. In comparison, the real difference between them is 11.2%. These differences were caused by the absence of a reference image and the used evaluation training set is not large enough.

In this context, it becomes possible to understand the reason for the contradictions between the results of previous studies (14,25-28), between those who confirm the importance of atmospheric correction in the classification process and those who deny it. This may often be due to the differences in the data used in terms of the characteristics of the satellite used (spatial and spectral resolution and number of bands), as well as the different study areas and classes they contain, and the diversity of algorithms used in processing.

## 4. Conclusion

The research results underscore the importance of selecting appropriate processing levels and

implementing effective atmospheric correction techniques in remote sensing classification tasks. Specifically, the superior performance of the C2L2 datasets, achieved through the LaSRC algorithm, significantly impacts dataset characteristics and leverages advanced preprocessing methods. in addition, the dominance of the SVM in effectively classifying remote sensing data highlights the need for careful evaluation of both processing levels and classifier types. This approach ensures accurate and reliable classification outcomes, leading to considerable improvements in classification accuracy and interpretation of remote sensing data. Furthermore, the variance in classification accuracy for different classes between different preprocessing levels makes it possible to obtain different results if the same previous steps are applied in other study areas with dissimilar classes or contain the same classes in different proportions. Finally, the confusion matrix results don't reflect the real variations in the result with the absence of a reference image, and enough training samples. In such cases, alternative evaluation methods are needed.

**Acknowledgment**

The researcher would like to express gratitude to the Department of Physics, College of Education for Pure Science (Ibn-Al-Haitham), University of Baghdad, for supporting the completion and carrying out of this research work.

**Conflict of Interest**

The authors declare that there are no conflicts of interest.

**Funding**

No funding.

**Ethical Clearance**

The project was approved by the local ethical committee at the University of Baghdad.

**References**

1. Liu X, He J, Yao Y, Zhang J, Liang H, Wang H, Hong Y. Classifying urban land use by integrating remote sensing and social media data. Int J Geogr Inf Sci. 2017;31(8):1675-1696. https://doi.org/10.1080/13658816.2017.1324976
2. Mahdi AS. The Land Use and Land Cover Classification on the Urban Area. Iraqi J Sci.2022; 63(10):4609-4619. https://doi.org/10.24996/ijs.2022.63.10.42
3. Chipman JW, Lillesand TM, Schmaltz JE, Leale JE, Nordheim MJ. Mapping lake water clarity with Landsat images in Wisconsin, USA. Can J Remote Sens. 2004;30(1):1-7. https://doi.org/10.5589/m03-047
4. Lamquin N, Woolliams E, Bruniquel V, Gascon F, Gorroño J, Govaerts Y, Leroy V, Lonjou V, Alhammoud B, Barsi JA. An inter-comparison exercise of Sentinel-2 radiometric validations assessed by independent expert groups. Remote Sens Environ. 2019;233:111369. https://doi.org/10.1016/j.rse.2019.111369
5. Pinto C, Ponzoni F, Castro R, Leigh L, Mishra N, Aaron D, Helder D. First in-flight radiometric calibration of MUX and WFI on-board CBERS-4. Remote Sens. 2016;8(5):405. https://doi.org/10.3390/rs8050405.

6. Hagolle O, Huc M, Pascual DV, Dedieu G. A multi-temporal and multi-spectral method to estimate aerosol optical thickness over land, for the atmospheric correction of FormoSat-2, LandSat, VENμS and Sentinel-2 images. Remote Sens. 2015;7(3):2668-2691. https://doi.org/10.3390/rs70302668
7. Maher A, Ghazal NK. Removing atmospheric effects for Multi spectral images (OLI 8) using ATCOR model. IOP Conference Series: Mater Sci Eng. . 2020 March; 757(1):012072. IOP Publishing. https://doi.org/10.1088/1757-899X/757/1/012072
8. Naji TA. New multispectral images classification method based on MSR and Skewness implementing on various sensor scenes. Iraqi J Sci .2015;56(3A):2104-2114. https://ijs.uobaghdad.edu.iq/index.php/eijs/article/view/9967
9. Gumma MK, Thenkabail PS, Hideto F, Nelson A, Dheeravath V, Busia D, Rala A. Mapping irrigated areas of Ghana using fusion of 30 m and 250 m resolution remote-sensing data. Remote Sens. 2011;3(4):816-835. https://www.mdpi.com/2072-4292/3/4/816
10. Townshend JR, Masek JG, Huang C, Vermote EF, Gao F, Channan S, Sexton JO, Feng M, Narasimhan R, Kim D, Song K, Song D, Peng Song X, Noojipady P, Tan P, Hansen MC, Li M. Wolfe R. E. Global characterization and monitoring of forest cover using Landsat data: opportunities and challenges. Int J Digit Earth. 2012;5(5):373-397. https://doi.org/10.1080 /17538947.2012.713190
11. Crawford CJ, Roy DP, Arab S, Barnes C, Vermote E, Hulley G, Gerace A, Choate M, Engebretson C, Micijevic E, Schmidt G, Anderson C, Anderson M, Bouchard M, Cook B, Dittmeier R, Howard D, Jenkerson C, Kim M, Kleyians T, Maiersperger T, Mueller C, Neigh C, Owen L, Page B, Pahlevan N, Rengarajan R, Roger JC, Sayler K, Scaramuzza P, Skakun S, Yan L, Zhang HK, Zhu Z, Zahn S. The 50-year Landsat collection 2 archive. Sci Remote Sens.. 2023;8:100103. https://doi.org/10.1016/j.srs.2023.100103
12. KC M, Leigh L, Pinto CT, Kaewmanee M. Method of Validating Satellite Surface Reflectance Product Using Empirical Line Method. Remote Sens. 2023;15(9):2240. https://doi.org/10.3390/rs15092240
13. Jin Y, Hao Z, Huang H, Wang T, Mao Z, Pan D. Evaluation of LaSRC aerosol optical depth from Landsat-8 and Sentinel-2 in Guangdong-Hong Kong-Macao greater bay area, China. Atmos Environ. 2022;280:119128. https://doi.org/10.1016/j.atmosenv.2022.119128
14. Muchsin F, Pradono KA, Prasasti I, Dianovita D, Ulfa K, Veronica KW, Novresiandi DA, Ibrahim A. Effect of atmospheric correction algorithm on landsat-8 and sentinel-2 classification accuracy in paddy field area Int J Remote Sens Earth Sci. 2023;20(1):58-66. http://dx.doi.org/10.30536/j.ijreses.2023.v20.a3845
15. Abdulwahab RA, Al-Ani LA, Shaban AH. Hyperspectral pansharpening improvement using MNF transformation. In: AIP Conf Proc. 2023 November; 3018(1). AIP Publishing. https://doi.org/10.1063/5.0171978
16. Pohl, C, Van Genderen JL. Review article multisensor image fusion in remote sensing: concepts, methods and applications. Int J Remote Sens. 2010;19(5),823-854.https://doi.org/10.1080/014311698215748
17. Ali SM, Mahdi AS, Tawfeeq RJ, Naji TA. Research Address: New Multispectral Image Classification Methods Based on Scatterplot Technique. Proceeding of 3rd scientific conference of the College of Science. University of Baghdad, Iraqi J Sci. 2009 March;773-780.
18. Naji TA, Hatem AJ. New adaptive satellite image classification technique for al Habbinya region west of Iraq. Ibn Al-Haitham J Pure Appl Sci.. 2013;26(2):143-149. https://jih.uobaghdad.edu.iq/index.php/j/article/view/494
19. Romaszewski M, Głomb P, Cholewa M. Semi-supervised hyperspectral classification from a small number of training samples using a co-training approach. ISPRS J Photogramm Remote Sens. 2016;121;60-76. https://doi.org/10.1016/j.isprsjprs.2016.08.011
20. Abduljabbar HM, Naji TA. separating the terrain cover of iraqi marshes region usinq new satellite band combination. Iraqi J Agric Sci 2020;51(6):1504-1516. https://doi.org/10.36103/ijas.v51i6.1178

21. De Jong SM, Van der Meer FD. Remote sensing image analysis: including the spatial domain. Springer Science & Business Meda. 2021;236(3):1-19.
22. Pal M, Foody GM. Feature selection for classification of hyperspectral data by SVM. IEEE Trans Geosci Remote Sens. 2010;48(5):2297-2307. https://doi.org/10.1109/TGRS.2009.2039484
23. Su J, Yi D, Liu C, Guo L, Chen WH. Dimension reduction aided hyperspectral image classification with a small-sized training dataset: experimental comparisons. Sensors. 2017;17(12):2726. https://doi.org/10.3390/s17122726
24. Zhang T, Su J, Liu C, Chen WH, Liu H, Liu G. In Band selection in sentinel-2 satellite for agriculture applications. 23rd Int Conf Autom Comput.. 2017;1-6. https://doi.org /10.23919/IConAC.2017.8081990
25. Lin C, Wu CC, Tsogt K, Ouyang YC, Chang CI. Effects of atmospheric correction and pansharpening on LULC classification accuracy using WorldView-2 imagery. Inf Process Agric. 2015;2(1):25-36. https://doi.org/10.1016/j.inpa.2015.01.003
26. Prieto-Amparan JA, Villarreal-Guerrero F, Martinez-Salvador M, Manjarrez-Domínguez C, Santellano-Estrada E, Pinedo-Alvarez A. Atmospheric and radiometric correction algorithms for the multitemporal assessment of grasslands productivity. Remote Sens. 2018;10(2):219. Available from: https://doi.org/10.3390/rs10020219
27. Lhissou R, El Harti A, Maimouni S, Adiri Z. Assessment of the image-based atmospheric correction of multispectral satellite images for geological mapping in arid and semi-arid regions. Remote Sens Appl: Soc Environ. 2020; 20: 100420. https://doi.org/10.1016 /j.rsase.2020.100420
28. Al-Doski J, Hassan FM, Norman M, Najim AA. Interaction of image fusion techniques and atmospheric correction for improve SVM accuracy. Earth Sci Informatics. 2022;15(4):2673-2687. https://doi.org/10.1007/s12145-022-00884-7
29. Rahman MM, Robson A. Integrating Landsat-8 and sentinel-2 time series data for yield prediction of sugarcane crops at the block level. Remote Sens. 2020;12(8):1313. https://doi/10.3390/rs12081313
30. Maciel DA, Pahlevan N, Barbosa CCF, de Novo EM, Paulino RS, Martins VS, Vermote E, Crawford CJ. Validity of the Landsat surface reflectance archive for aquatic science: Implications for cloud-based analysis. Limnol Oceanogr Lett. 2023; 8(6):850-858. https://doi.org/10.1002 /lol2.10344
31. Obaid OH, Abdulameer IMA. Turbidity Changes in the Tigris River Using Satellite Data During the COVID-19 Related Lockdown. Ibn Al-Haitham J Pure Appl Sci. 2022;35(4): 76-82. https://doi.org/10.30526/35.4.2874
32. Niroumand-Jadidi M, Bovolo F, Bresciani M, Gege P, Giardino C. Water quality retrieval from landsat-9 (OLI-2) imagery and comparison to sentinel-2. Remote Sens. 2022;14(18):4596. https://doi.org/10.3390/rs14184596
33. Micijevic E, Barsi J, Haque MO, Levy R, Anderson C, Thome K, Czapla-Myers J, Helder D. Radiometric performance of the Landsat 9 Operational Land Imager over the first 8 months on orbit. In Earth Observing Systems XXVII. 2022 September; 12232: 249-256. SPIE.
34. Choate MJ, Rengarajan R, Storey JC, Lubke M. Landsat 9 geometric characteristics using underfly data. Remote Sens. 2022;14(15):3781. https://doi.org/10.3390/rs14153781
35. Wulder MA, Roy DP, Radeloff VC, Loveland TR, Anderson MC, Johnson DM, Healey S, Zhu Z, Scambos TA, Pahlevan N, Cook BD. Fifty years of Landsat science and impacts. Remote Sens Environ.2022;280:113195.https://doi.org/10.1016/j.rse.2022.113195
36. Masek JG, Wulder MA, Markham B, McCorkel J, Crawford CJ, Storey J, Jenstrom DT. Landsat 9: Empowering open science and applications through continuity. Remote Sens Environ.. 2020;248:111968. https://doi.org/10.1016/j.rse.2020.111968
37. Mohammed MA, Naji TA, Abduljabbar HM. The effect of the activation functions on the classification accuracy of satellite image by artificial neural network. Energy Procedia. 2019;157:164-170. https://doi.org/10.1016/j.egypro.2018.11.177

38. Kaduhm HS, Abduljabbar HM. Studying the classification of texture images by K-means of co-occurrence matrix and confusion matrix. . Ibn Al-Haitham J Pure Appl Sci.2023;36(1):113-122. https://doi.org/10.30526/36.1.2894
39. Majed M, AbdulJabbar HM. The Change in the Land Cover of Mahmudiyah City in Iraq for the Last Three Decades. . Ibn Al-Haitham J Pure Appl Sci. 2022;35(3):44-55. https://doi.org/10.30526/35.3.2831
40. Khudair BH, Ali SK, Jassim D. T. Prediction of Municipal Solid Waste Generation Models Using Artificial Neural Network in Baghdad city, Iraq. J Eng. 2018;24(5):113-123. https://doi.org/10.31026/j.eng.2018.05.08
41. Suhaili RH, Nasser NO. Water quality indices for Tigris river in Baghdad city. J Eng. 2008;14(03):2656-2668. https://doi.joe.uobaghdad.edu.iq.
42. Saleh S. A. Impact Of Urban Expansion On Surface Temperature In Baghdad, Iraq Using Remote Sensing And Gis Techniques. Al-Nahrain J Sci 2010;13(1):48-59. https://doi.org/10.22401/JNUS.13.1.07